International Journal of Engineering Trends and Technology
ISSN: 2231–5381 / https://doi.org/10.14445/22315381/IJETT-V72I9P112

Volume 72 Issue 9, 139-153, September 2024

Review Article

Recent Advances in the Development of Organic Solar Cells and Perovskite Solar Cells

Ho Soonmin[1], Md. Hojaifa Daiyan Chowdhury[2], Muhammad Rashique Hamjah Chowdhury[3], Md. Iqbal Bahar Chowdhury[4]

[1]*Faculty of Health and Life Sciences, INTI International University, Putra Nilai, Negeri Sembilan, Malaysia.*
[2,3,4]*School of Science and Engineering, United International University, Dhaka, Bangladesh.*

[1]*Corresponding Author : soonmin.ho@newinti.edu.my*

Received: 01 April 2024 Revised: 16 July 2024 Accepted: 27 August 2024 Published: 28 September 2024

Abstract *- Organic and Perovskite Solar Cells (OSCs and PSCs) are based on solution-processable semiconductors, whereas Si-based Solar Cells (SSCs) are based on silicon wafers, which require costlier pure silicon materials because of their high-temperature production. OSCs are light in weight and environmentally friendly. In addition, researchers found that light absorbers were available in a wide range of colors. In contrast, PSCs yielded higher* conversion efficiency *due to excellent charge-carrier mobilities, lifetime and light absorption. In this work, various types of techniques have been used to study the properties of the prepared materials. The obtained results showed that photovoltaic parameters are strongly depending on experimental conditions.*

Keywords *- OSCs, PSCs, Photovoltaic, Energy efficiency, Energy consumption, Clean energy technology.*

1. Introduction

The sun, an energy-supplier of 4 million exajoule per year to the earth, [1] is the most plentiful and harmless resource of energy. [2] The solar energy obtained per hour is greater than that used per year. [3] Hence, the photovoltaic (PV) cells that can harvest this solar energy become increasingly crucial for environment-friendly carbon neutralization [4] to combat the climactic change due to global warming. The total capacity of solar panels installed till 2021 approached 866 GW (28% of the total global capacity), [4] which is projected to exceed 4500 GW by 2050. [5–7] This sky-rocketing increase in PV capacity is due to the more practical viewpoint, extended lifetime, and reduced cost of maintenance [8] and also due to the rapidly growing building applied and integrated PV (BAPV & BIPV) installments in the urban environment. [9, 10] Several generations (1G, 2G, 3G) have been observed in PV technology. The 1G solar cells (SCs) use crystalline silicon (Si), the 2G SCs (thin-film SCs) use amorphous and polycrystalline semiconductors such as CdTe, CIGS and GaAs [11], and the 3G SCs use solution-processable organic and perovskite semiconductors. [12] Both OSCs and PSCs increasingly draw the scientific community as potential candidates to replace SSCs for the forthcoming low-cost PV technology. SSCs employ the energy-intensive Czochralski process to produce pure Si [11] and, hence, require costlier, high-temperature production. [13] In contrast, both OSCs and PSCs employ a low-energy roll-to-roll manufacturing process [14], which enables low-cost fabrication. In the visible spectrum, both organic and perovskite semiconductors have a higher absorption coefficient than that of Si, [15] for which OSCs and PSCs need less material than SSCs, reducing their cost and weight. Under reduced solar irradiation, the Power Conversion Efficiency (PCE) for SSCs decreases, whereas that for both OSCs and PSCs increases, [12] making them appropriate for indoor applications. Moreover, both OSCs and PSCs can be used in portable and wearable electronics due to their fabricability on flexible substrates. [14] OSCs are a superior choice for indoor and IoT applications; [16] PSCs are used for BIPV applications. [13] In recent years, the performance improvement of both OSCs and PSCs has progressed very rapidly. The PCE of the latest OSCs and PSCs exceeds the limit of 18% and 25%, respectively. The exceptional advancement of these solar cells can be attributed to the different technological improvement, which includes improved structural design, improvement in the electronic and optical properties through the morphological design of photoactive material, performance improvement of Hole Transport Layer (HTL) and Electron Transport Layer (ETL) with doping and/or additives, and appropriate choice of metal contacts. This work briefly reviews the recent technologies employed for the rapid advancement of both OSCs and PSCs. In section 2, the structure and working principle are discussed. Section 3 gives an overview of the intrinsic material properties of the photoactive materials. Section 4 discusses the cell development for OSCs and PSCs, which includes the morphological development of active layers as well as the

improved design of HTLs and ETLs. Finally, the concluding remarks are drawn, pointing out the future development of these solar cells.

2. Structure and Working Principle

The device architectures for both OSCs and PSCs are very similar. Both use similar Charge Transport Layers (CTL) and metal contacts. The difference lies in the photoactive layer. As photoactive layer materials, OSCs use conjugate polymers or fullerene/non-fullerene derivatives, and PSCs use perovskites.

2.1. OSC Structure and Working Principle

Conjugate polymer-based OSCs technology is an increasingly promising third-generation technology because of its low-cost materials, solution-processable, low-cost fabrication process, [17] semi-transparent, flexible, and lightweight structure. Although the first OSC [18] had a PCE of < 1%, modern OSCs surpass the PCE limit of 18 %, keeping pace with the rapid technological advances in device architecture, morphology, and material design. [19] The structures of OSCs [Figures 1(A-D)] can be categorized into single-layer (SL), bi-layer (BL), and Bulk Heterojunction (BHJ). In OSCs, the two electrodes' work function difference develops an electric field (E_{bi}), [20] which separates the excitons photogenerated in the photoactive layer, where the photoactive layer is sandwiched between the electrodes. As photoactive layer, single-layer OSCs use only one organic semiconductor, while the bilayer uses a heterojunction of electron donor/acceptor (D/A) type organic semiconductors. The PCE of a single layer is very low (< 0.1% for p-phenylene vinylene-based organic solar cell [21]) because of insufficient E_{bi} to separate the excitons into electron-hole pairs.

The excitons generated in the bilayer can be separated into electron-hole pairs by an additional field developed at the D/A interface [22]. Hence, these OSCs show a higher PCE than that of a single layer. However, the separated electrons (holes) are recombined due to the poor diffusion length of the conjugated polymers (only 4-20 nm [23]) as they move closer to the respective electrode, thereby limiting the PCE of the bilayer. [24]

In BHJ OSCs, a blend of D/A materials [25] is employed to increase the diffusion length, which enhances PCE. The PCE can be further enhanced by employing CTLs (ETL and HTL) to decrease the recombination near the electrodes, where ETL (HTL) is the electron (hole) transport layer that boosts the electron (hole) transport and blocks the hole (electron) transport towards the respective electrode. However, the placement of the cathode on top of the photoactive layer requires vacuum steps, [26] for which the fabrication is not fully solution-processed and hence poses a severe bottleneck for large-scale fabrication. A regular BHJ (n-i-p type) needs to be flipped to the inverted one (p-i-n type) to avoid vacuum processing steps and afford fully solution-processed large-scale production. [27]

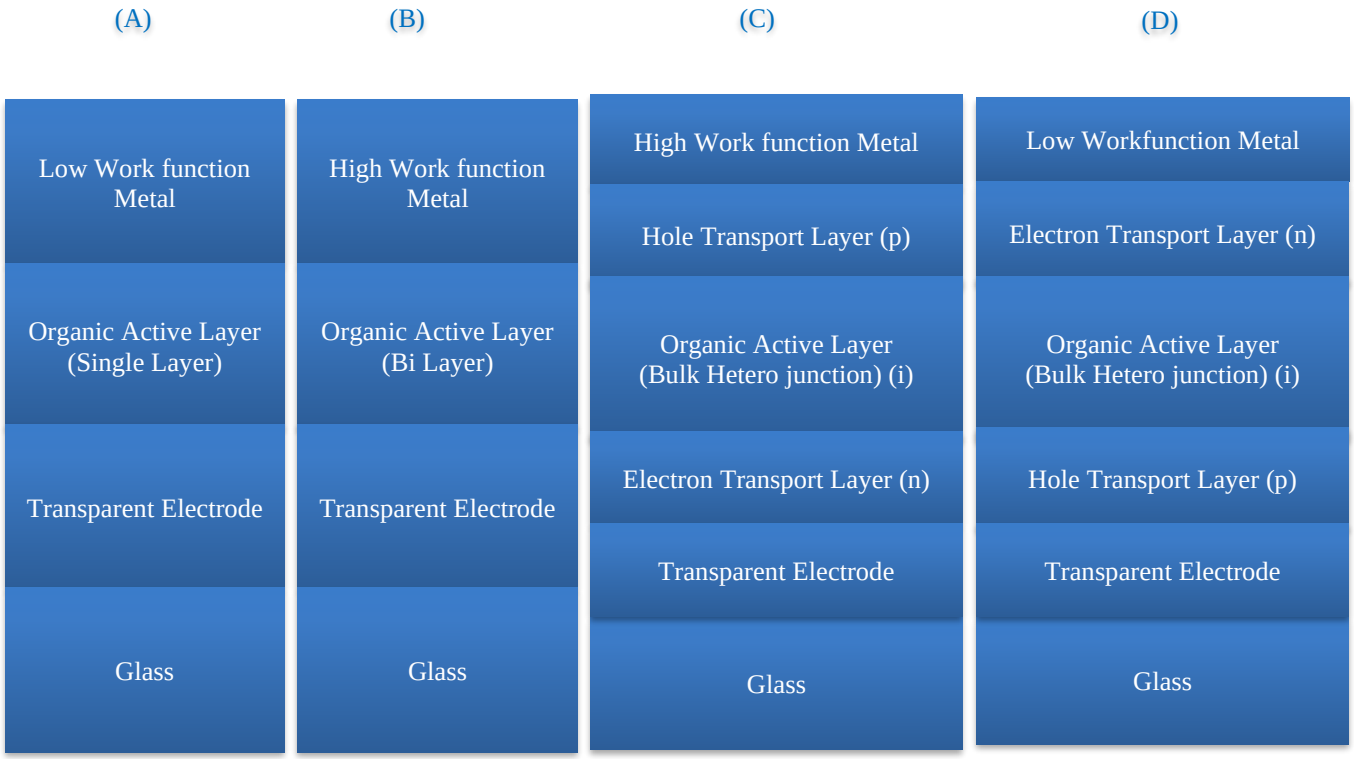

Fig. 1 OSC Structures: (A) Single layer, (B) Bilayer, (C) Inverted BHJ. and (D) Regular BHJ

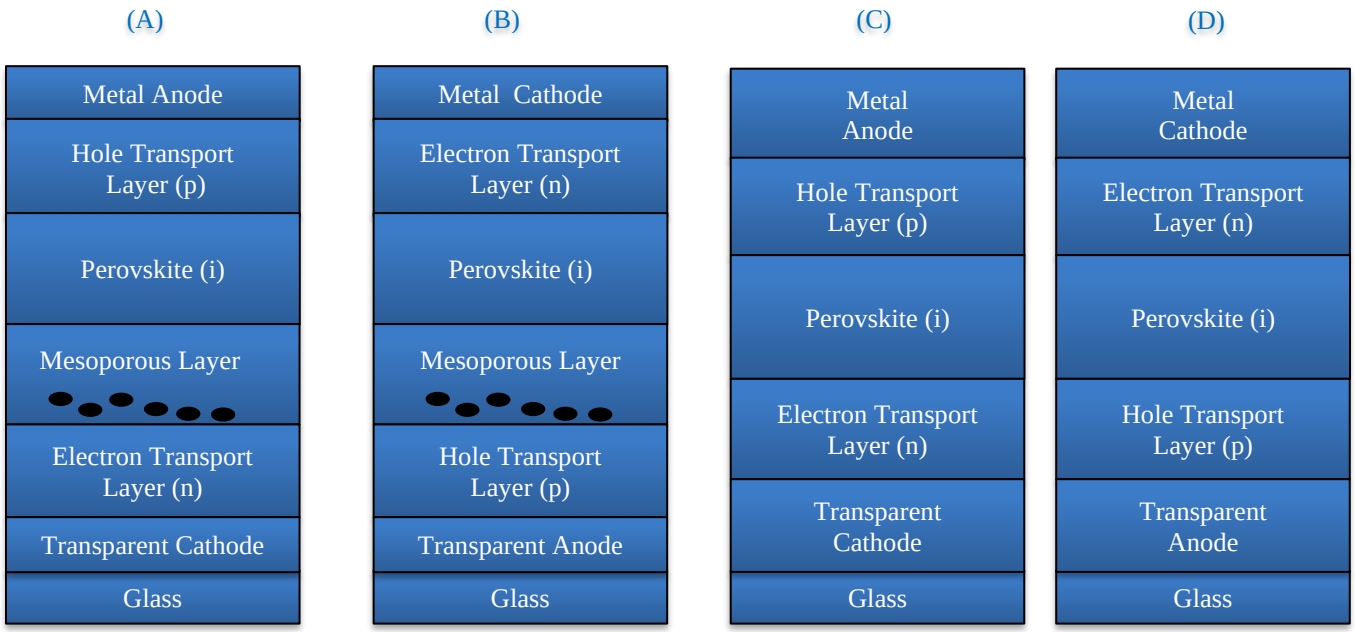

Fig. 2 PSC structures: (A) Inverted mesoscopic, (B) Regular mesoscopic, (C) Inverted planar, and (D) Regular planar

2.2. PSC Structure and Working Principle

Perovskite semiconductor-based solar cell technology has become the fastest-growing third-generation technology, where PCE has been observed to rise from 3.8% to 25.73% since its inception in 2009. [28] This steep rise in efficiency can be attributed to their superb structural (higher crystallinity, ionicity, and defect tolerance), electronic (higher relative permittivity, lower exciton binding energy, [29] higher charge carrier mobility, and larger carrier diffusion length), and optical (higher absorption ability) properties. [30] PSCs can be categorized into two groups, namely mesoscopic and planar, where both are of regular n-i-p and inverted p-i-n types [Figures 2 (A-D)]. A typical mesoscopic regular (inverted) structure consists of a metal anode (cathode), the HTL (ETL), the photoactive perovskite layer, a thin mesoporous layer (TiO_2, Al_2O_3), and a transparent conductive cathode (FTO, ITO glass) in Figures 2 (A, B).

Planar regular (inverted) structure [Figures 2(C, D)] is a mesoscopic counterpart without having any mesoporous layer. Although the mesoporous layer requires high-temperature processing, for which the mesoporous structure is inappropriate for flexible panels, this layer ensures improved film quality and morphology control as well as device repeatability. The HTL in most PSCs is used to prevent interfacial charge compounding, [31] which enhances charge collection, thereby increasing the V_{oc} and PCE.

3. Intrinsic Properties of Photoactive Layer

The intrinsic material properties of photoactive layers of organic and PSCs are quite different, resulting in their obviously different performance. [32] These intrinsic (electronic and optical) properties are listed in Table 1.

3.1. Structural Properties

The structural unit of organic semiconductors is formed with carbon-hydrogen atoms (grouped together by relatively weaker van der Waals bonds). It belongs to the monoclinic or triclinic class of crystals if crystallized. [33] Based on the molecular weight of the constituents, organic semiconductors are mainly categorized as either conjugate polymers or small molecules, where molecular weights are distributed in the former and small and precise for the latter. [34] Solution processes can be used for conjugated polymer preparation. Thermal evaporation is used to deposit small molecules, and solution processing can be used to fabricate small molecules by tailoring their chemical structure.

Perovskite semiconductors ($CaTiO_3$ mineral) have a generic chemical structure ABX_3, [35] where A site is occupied by methylammonium (MA^+)/ formamidinium (FA^+)/caesium (Cs^+)-based monovalent, large-radius cations, B site by Pb_2^+/Sn_2^+-based divalent, small-radius metallic cations and X site by monovalent halide (Cl^-/Br^-/Cl^-/I^-) anion. The crystal structure of perovskite can be cubic, tetragonal, or orthorhombic based on crystallinity. [36]

3.2. Electronic Properties

Because of the relatively weaker van der Waals bonding, OSCs such as conjugate polymers are soft materials [37], whereas most PSCs are direct bandgap semiconductors. [38] In comparison with perovskites, thin films of conjugate polymers are less crystalline and less ionic, for which the dielectric constant of conjugate polymers (ε_r = 2−4) is significantly lower than that of perovskites (ε_r = 20−50). [39] Hence, the electron/hole Coulombic interaction in conjugate polymer is stronger than in perovskites. [40]

Table 1. Summary of structural, electronic, and optical properties of OSCs

Properties	OSCs	PSCs
Structural		
Crystallinity	less crystalline	highly crystalline
Ionicity	less ionic	more ionic
Degree of electron/phonon coupling	High	Lower
Structural and energetic disorder	Higher	Lower
Delocalization of excited states	Lower	Higher
Electron-hole interactions	Large	Weaker
Electronic		
Optical bandgap, E_{gopt} (eV)	1.0-1.6	1.4-1.6
Relative Dielectric constant, ε_r	poor (2.0-4.0)	high (20-50)
Exciton Binding Energy, E_b (meV)	> 100	< 25
Effective carrier mobility, μ ($cm^2V^{-1}s^{-1}$)	10^{-5} –10^{-4}	0.1-10
Effective carrier lifetime, τ (μs)	1-100	10-100 times faster than OSC
Effective mobility-lifetime product, $\mu\tau$	10-100 times smaller	10-100 times larger
Carrier diffusion length (nm)	≈ 20	> 500
Coulomb capture radius, r_C (nm)	> 15	< 2
Optical		
Absorption Coefficient, α (cm^{-1})	> 10^5	> 10^5

The photoexcitation generates rigidly bound electron-hole pairs (Frenkel excitons) in organic semiconductors due to lower ε_r value. Weakly-bound EHPs (Wannier-Mott excitons) were observed in perovskite due to higher ε_r value. [41] For neat conjugate polymers, the Frenkel excitons have a shorter exciton lifetime (≈ 20 ps−1 ns) and exciton diffusion length (≈ 3−20 nm). Also, due to lower ε_r, the electron-phonon coupling in conjugate polymer is relatively stronger, for which more phonon modes and more excited states are observed in conjugate polymer than their perovskites counterparts. Moreover, structural and energetic disorders are stronger in conjugated polymers than in perovskites, leading to more localization of excited states in conjugate polymers. The effective carrier mobility (μ) observed in perovskites (0.1–10 $cm^2V^{-1}s^{-1}$) is ≈ 10^3 faster than that in conjugate polymers (10^{-5} − 10^{-4} $cm^2V^{-1}s^{-1}$). The dominant band-like transport with low effective mass [42] increases the carrier mobility in perovskites. On the other hand, hopping-like transport with small polarons reduces the carrier mobility in organic semiconductors. The perovskites in PSCs show a 1-2 order faster effective carrier lifetime (τ) than that of blended organic semiconductors in OSCs, implying a 10-100 times faster bimolecular recombination rate in PSCs [43,44]. Finally, the effective carrier mobility-lifetime product ($\mu\tau$) in PSCs is larger than that in OSCs (as μ ≈ 10^3 larger and τ = 10^{-1} − 10^{-2} smaller than those of organic semiconductors). The larger $\mu\tau$ results in a larger carrier diffusion length in PSCs, which extracts the charges efficiently in PSCs driven only by the diffusion transport, even with a thicker active layer.

3.3. Optical Properties

Both OSCs and PSCs have a similar capability of efficient light absorption in the vis-NIR region of the solar spectrum with 100-500 nm thin active layers owing to their higher absorption coefficient (> 10^5 cm^{-1}). Organic blends [45] exhibit stronger absorption in the visible/near-IR spectrum, whereas perovskites show the same in the blue/UV spectrum. In order to achieve higher PCE, in most bulk hetero junction OSCs, active layer thickness (t_{act}) should be within 100 nm (t_{act} ≤ 100 nm). When t_{act} > 100 nm, recombination loss increases, and the limiting efficiency value in OSCs increases. [46] PSCs demonstrate a higher efficiency [47] for t_{act} > 500 nm, as their higher carrier mobility enhances higher charge extraction. [48] Therefore, the differences in photophysics involved in efficient photo absorption set the limit of t_{act} ≈ 100 nm for organic and within 200-700 nm for PSCs. [49]

4. Cell Development

Although both OSCs and PSCs are based on solution-processable semiconductors [12] and both use similar device architecture, the cell development, i.e. fabrication methods for these solar cells, are completely different. This is due to the difference in the photoactive material properties, and hence, the HTL and ETL used in each cell need different treatment of fabrication methods to achieve improved performance metrics.

4.1. OSC Development

OSCs are considered eco-friendly energy solutions [50]; however, their demonstrated lower PCE is due to lower charge diffusion length and inadequate light absorption. OSCs have been modified via several channels, such as controlling the morphology, [51] incorporating nanoparticles (NPs) into active layers, and reconfiguring optical device structure. [52]

4.1.1. D/A Interface Engineering

In the early days, the BHJ OSCs blended Fullerene Derivative Acceptors (FDAs) such as $PC_{61}BM$ $PC_{71}BM$ with conjugate polymer donors (CPDs) such as P3HT to improve the D/A interface and, hence, the PCE. Reported PCEs for

these OSCs are 3.5% [53] and 4.1% [54]. Constant research efforts led to the use of alternative FDAs, for example, F1 [55], $NC_{61}BM$ [56], $bisPC_{61}BM$ [57], F [58], ICBA [59, 60] and $IC_{70}BA$ [61]. The increased LUMO level of these FDAs w.r.t. PCBM increases both V_{OC} and FF and, hence, the PCE. Table 2 shows this increasing trend, where the highest V_{OC} of 0.84 V and the highest PCE of 6.48% are observed for ICBA-based FDA [61]. As a CPD, although P3HT is widely used, it suffers from the absorption-spectra mismatch with FDAs due to its higher bandgap, resulting in lower J_{sc}.

To increase the absorption (hence, to increase J_{sc} and PCE), various narrow-bandgap polymer donors like PTB1 [62], PCPDTBT [63], PTB4 [64], PTB7 [65], PTB7-Th [66, 67], PBDTTT-CF [68], PffBT4T2OD [69] and PffBT4T-C9C13 [70] are reported in the literature. As shown in Table 3, the PffBT4T-C9C13/ $PC_{71}BM$ CPD/FDA-based OSC shows J_{SC} = 20.2 mA/cm^2 and PCE =11.7%. [70] Small Molecular Non-Fullerene Acceptors (SM NFAs) demonstrate stronger absorbance [71] due to their narrower bandgap than FDAs, which are excellent choices as acceptor material.

SM NFAs are flexibly synthesised with rigid A-D-A backbone for improved conjugation and demonstrate easily-tunable, extended absorption spectrum (to near-infrared region) and enhanced charge transfer. [72] Numerous SM NFAs such as IDIC [73], ITIC [74], IOIC3 [75], SeTIC4Cl [76], Y6 [77, 78], Y6Se [79], m-BTP-PhC6 [80], BTP-eC9 [81] and L8BO [82] are some examples of SM NFAs reported in the literature. Table 4 lists the performance metrics of these SM NFAs. The highest PCE of 18.6% is obtained for L8-BO [82], as shown in Table 4.

4.1.2. Development of HTL through additives

For OSCs, PEDOT: PSS has gained more attention in the scientific community as a better choice of HTL because of its simple processing, higher transparency, ecofriendly solvent, and higher electrical conductivity. Continuous research efforts have been conducted in the literature to enhance the functionality of PEDOT: PSS by adding different NPs to achieve higher PCE of OSCs. Alkhalayfeh and co-workers [83] demonstrated that spiky durian-shaped NPs can be added into PEDOT: PSS to improve cell performance (Table 5).

The size properties (50 nm to 55 nm) and surface morphology have been studied using FESEM (homogeneous without agglomeration), TEM method (durian-shaped) (Figure 3a) and AFM technique (Figure 3b) (surface roughness= 8.1 nm to 11.6 nm). The enhancement of performance metrices (PCE, J_{sc}, FF and V_{oc}) has been observed with an increasing proportion of Au@Ag NPs in films, as the NPs help reduce the scattering mechanism of the incident light. The best performance metrices have been observed for 14% Au@Ag NPs (J_{sc} = 18.98 mA/cm^2, V_{oc} = 699.1 mV, FF = 31.4% and PCE = 4.15%, as seen in Table 5). However, increasing the proportion by more than 14%, the NPs become less effective in reducing the scattering of the incident light, thereby causing less light absorption (less J_{sc}) and increased recombination (less V_{oc} and FF), for which performance metrices of OSCs become degraded.

Table 2. Performance metrics of P3HT-based OSCs with different FDAs

FDA	$PC_{61}BM$	$PC_{71}BM$	F1	$NC_{61}BM$	$bisPC_{61}BM$	F	ICBA	ICBA	$IC_{70}BA$
Ref.	[53]	[54]	[55]	[56]	[57]	[58]	[59]	[60]	[61]
PCE (%)	3.5	4.1	3.7	4.09	4.5	5.25	5.44	6.48	5.79
FF (%)	60	55	60.3	64	68	63	67	72.7	63
V_{oc} (V)	0.55	0.61	0.564	0.7	0.724	0.81	0.84	0.84	0.81
J_{sc} (mA/cm^2)	8.5	12.2	10.8	9.06	9.14	10.3	9.67	10.61	11.34

Table 3. Performance metrics of OSCs with different NBG polymer donors

NBG PD	PTB1	PCPDTBT	PTB4	PTB7	PTB7-Th	PTB7-Th	PBDTTT-CF	PffBT4T-2OD	PffBT4T-C9C13
Acceptor	$PC_{71}BM$	$PC_{71}BM$	$PC_{61}BM$	$PC_{71}BM$	$PC_{71}BM$	$PC_{71}BM$	$PC_{71}BM$	$TC_{71}BM$	$PC_{71}BM$
Ref.	[62]	[63]	[64]	[65]	[66]	[67]	[68]	[69]	[70]
PCE (%)	5.3	5.5	5.9	9.21	9.35	10.1	7.73	10.8	11.7
FF (%)	63.3	55	61.4	69.99	74.3	66.9	66.9	75	74
V_{oc} (V)	0.56	0.62	0.74	0.754	0.8	0.775	0.76	0.77	0.788
J_{sc}(mA/cm2)	15	16.2	13	17.46	15.73	19.47	15.2	18.8	20.2

Table 4. Performance metrices of OSCs based on SM NFAs

SM NFA	IDIC	ITIC	IOIC3	SeTIC4Cl	Y6	Y6	Y6Se	m-BTP-PhC6	BTP-eC9	L8-BO
PD	FTAZ	PBDTS-TDZ	PTB7-Th	PM6	PM6	D18	D18	PTQ10	PM6	PM6
Ref.	[73]	[74]	[75]	[76]	[77]	[78]	[79]	[80]	[81]	[82]
J_{sc} (mA/cm^2)	20.8	17.78	22.9	22.92	27.43	27.7	27.98	25.3	26.2	26.03
V_{oc} (V)	0.84	1.1	0.762	0.78	0.845	0.859	0.839	0.883	0.839	0.893
FF (%)	71.8	65.4	74.9	75	73.8	76.6	75.3	79.3	81.1	80
PCE (%)	12.5	12.8	13.1	13.32	17.1	18.22	17.7	17.7	17.8	18.6

Table 5. Effect on performance metrices of OSCs based on PEDOT: PSS HTL with Au@Ag NPs

Proportion of NPs	PCE (%)	FF (%)	V_{oc} (V)	J_{sc} (mA/cm^2)
0%	2.5	30.9	0.6858	11.82
8%	3.6	31.2	0.6964	16.58
10%	3.73	31.3	0.6975	17.07
12%	3.84	31.3	0.6980	17.62
14%	4.15	31.4	0.6991	18.98
16%	4.02	31.2	0.6986	18.46

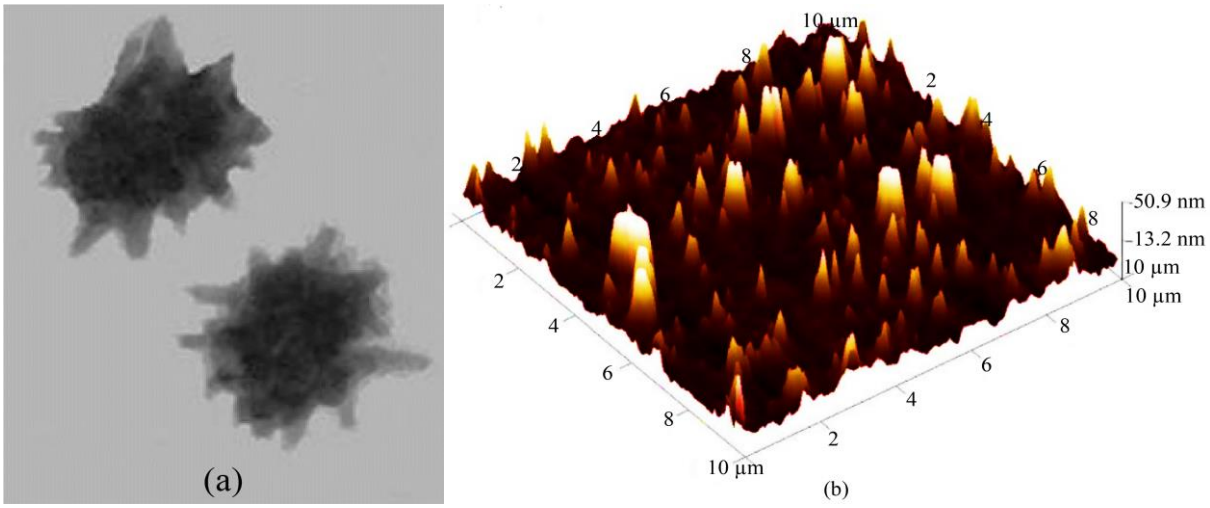

Fig. 3 (a) TEM and (b) AFM images [83]

Table 6. Effects on PCE of OSCs with ZnO ETL for UV-ozone treatment and Al-doping process

OSC	UV-ozone	Aluminum-doping (%)	PCE (%)
P3HT: PCBM	0	0%	1.67
	0	3%	1.85
	20	0%	1.83
	20	3%	2.32
J71:m-ITIC	0	0%	5.48%
	0	2%	6.41%
	20	0%	8.17%
	20	2%	9.47%

4.1.3. Development of ETL through Additives

In OSCs, zinc oxide (ZnO) is the widely used ETL for its air-stability, low-cost and higher electron mobility. However, improvement of the ZnO layer in different OSCs for higher PCE has been demonstrated via UV-ozone and aluminum doping process. [84] UV-ozone decreases the interfacial traps, reducing the recombination (increases V_{OC} and FF) and leakage current (increases J_{sc}). As a result, the PCE has increased from 1.67% to 1.83% in fullerene-based (P3HT: PCBM) OSC and from 5.48% to 8.17% in non-fullerene-based (J71:m-ITIC) OSC (Table 6). Based on the morphological studies, a small amount of aluminum (Al) doping to the ZnO samples ensures a smooth surface, smaller size, and uniform morphology with fewer pinholes, for which PCE can be improved irrespective of the UV-ozone treatment (Table 6). From Table 6 it can be observed that a 2% Al-doped, UV-ozone treated ZnO can boost the PCE of J71:m-ITIC OSC from 8.17% to 9.47% (15.91% increase) and a 3% Al-doped, UV-ozone treated ZnO can increase the PCE of P3HT: PCBM OSC from 1.83% to 2.32% (26.78% increase). It is noteworthy that the increase in PCE due to the Al-doping process is more significant in fullerene-based OSCs, implying its greater impact on achieving better morphological improvement in these OSCs.

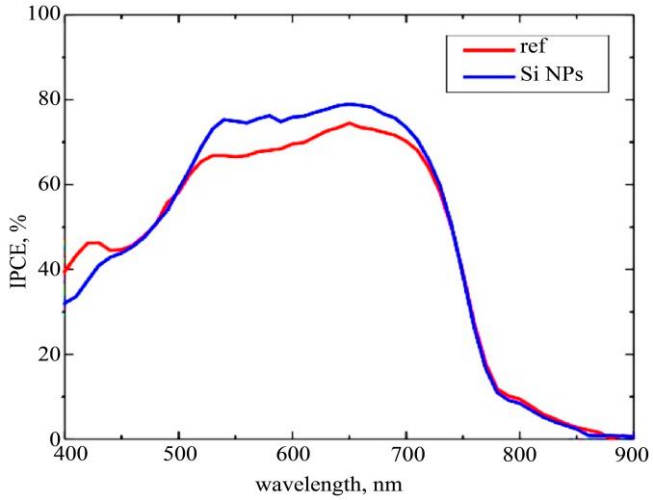

Fig. 4 Experimentally measured IPCE of an OSC with and w/o Si NPs [85]

4.1.4. Effects of Silicon NPs as Additives

Studies [85] show that silicon (Si) NPs as additives can significantly enhance the PCE of the OSCs. A laser ablation technique [85] has been employed to synthesize these resonant Si NPs. These NPs are spherical-shaped with a size of 150 nm. A significant improvement of PCE from 6% to 7.5% (i.e., a 25% increase) has been reported with Si NPs in the optimized conditions. This enhancement of PCE can be attributed to very strong light localization in the devices due to the presence of Si NPs. From experimental plots, as shown in Figure 4, [85] higher incident photon-to-current efficiency (IPCE) has been observed for the presence of Si NPs in the specific wavelength zone (525-725 nm), which is of great interest for solar cells.

In this wavelength zone, an IPCE of ≈ 75% has been observed due to the presence of Si NPs (Figure 4) as compared to the IPCE of 70% obtained when Si NPs are employed. These experimental results support the important role of Mie resonances (Si NPs) in OSC devices for stronger light localization.

4.2. PSC Development

PSCs are expected to replace Si-based solar cells in the future [86] because of their lower costs, simple production process, [87] greater flexibility, and excellent tolerance of defects in the structure. [88] Currently, there are several manufacturers, such as LG, Kao, Sekisui Chemical, BASF, Oxford Photovoltaics, Fujifilm Holdings, Hee Solar and Hunt Consolidated, that have engaged in the development of this technology.

4.2.1. Lead-based PSC Development

The spin coating technique has been used to prepare lead-based perovskite materials, as reported by Kanij and co-workers. [89] Morphology and structure of the $CH_3NH_3PbI_3$ ($MAPI_3$), $CH_3NH_3PbCl_3$ ($MAPCl_3$), $CH_3NH_3PbI_2Cl$ ($MAPI_2Cl$) and $CH_3NH_3PbICl_2$ ($MAPICl_2$) were studied using SEM and XRD, respectively. The obtained results reflected that all samples are tetragonal structures with fine crystallinity.

The variation of lattice parameters and, hence, that of the unit cell is due to the variation of halide ions (Table 7). Analysis of the SEM images, reported in [89], revealed that micro rods had been changed to microcube when the iodine was replaced with chlorine ion. In addition, higher DMF should be employed to enhance the film coverage.

Table 7. XRD studies of the prepared materials

Parameter	$MAPI_3$	$MAPI_2Cl$	$MAPICl_2$	$MAPCl_3$
2θ (degree)	14.47 28.85 32.22	11.01 13.12 31.93 39.13 52.55	14.38 28.56	16.03 31.89
FWHM (degree)	0.345 0.53 0.35	0.21 0.294 0.245 0.327 0.338	0.26 0.261	0.171 0.22
Crystallite size (nm)	20.77	30.18	31.11	42.23
Dislocation densit (nm^{-2})	0.0023	0.0011	0.0010	0.0005
Cell volume ($Å^3$)	165.86	362.14	59.86	200.93
Lattice parameters (Å)	a=6.134 b=6.134 c=4.409	a=13.509 b=13.509 c=3.335	a=3.122 b=3.122 c=6.142	a=4.254 b=4.254 c=11.103

Table 8. Performance metrices of PSCs with different doped-ETLs

ETL	TiO_2					SnO_2			ZnO	
Doping	Mg	Ce	Li	Zn	Zr	Cl	Zr/F	Ta	Mg	PbS
Ref.	[90]	[91]	[92]	[93]	[94]	[95]	[96]	[97]	[98]	[99]
PCE (%)	14.65	16.18	17.59	17.6	18.16	18.94	19.19	20.8	13.52	20.53
FF (%)	60.9	69	69.9	73.4	71.6	73	71.2	78.6	65	79
Voc (V)	1.08	1.07	1.101	1.1	1.076	1.07	1.105	1.161	0.83	1.14
Jsc (mA/cm^2)	22.27	21.95	22.86	21.83	23.57	24.25	24.39	22.79	25.06	22.8

4.2.2. Development of ETL through doping

In PSCs, ETL serves the role of electron extraction and hole blocking to achieve higher PCE. Metallic oxides, i.e. ZnO, tin oxide (SnO_2) and titanium oxide (TiO_2), are preferrable ETLs for PSCs due to their outstanding electronic and optical properties and affordable processing [29]. Of these, TiO_2 is most attractive in mesoscopic PSCs due to its ability to form dense and mesoporous layers [29] and also its larger band gap (about 3.7 eV), excellent environmental stability, good optical transparency, and excellent electron mobility. FTO-coated glass is usually employed as the top contact because of its lower sheet resistance and higher transparency.

However, severe recombination between the perovskite films and the FTO electrode happens in the presence of pinholes in TiO_2 layers, causing poor performance of the PSCs. Therefore, various metals like Mg [90], Ce [91], Li [92], Zn [93], Zr [94], etc. are doped with TiO_2 to increase the PCE further (Table 8). Zr-doped TiO_2-based PSC has achieved a PCE of PCE of 18.16% (Table 8). [95] To achieve higher PCE, Cl [95], Zr/F [96], Ta [97], etc., are doped with SnO_2-based ETL and Mg [99], PbS [99] etc., with ZnO-based ETL. PCEs of 20.8% and 20.53% have been reported for PSCs based on Ta-doped SnO_2 [97] and PbS-doped ZnO [99], respectively (Table 8).

4.2.3. Development of ETL through additives

Gang and co-workers [100] conducted a rigorous investigation to study the effects of PCBM-modified TiO_2 as ETL on the experimentally fabricated PSCs based on the n-i-p architecture. They also studied the effects of spin coating speed on the performance of PSCs and observed a decrease in FF and PCE when spin coating speed increases from 4000 rpm to 6000 rpm (Table 9). They attributed this degradation to the increase in series resistance with the spin coating speed. Table 9 also reveals that both FF and PCE values are lower for TiO_2 samples irrespective of the spin coating speed; however, PCBM-modified TiO_2 samples show higher FF and, hence, higher PCE values. TiO_2 (4000 rpm) samples show a PCE of 10.81%, whereas PCBM (2000 rpm)-modified TiO_2 (4000 rpm) sample shows a PCE of 13.42% (24.14% increase).

Table 9. PV performance of PSCs with PCBM-modified TiO_2 as ETL for varying spin coating speeds

ETL	J_{sc} (mA/cm^2)	FF (%)	PCE (%)
TiO_2 (2000 rpm)	17.09	57	7.9
TiO_2 (4000 rpm)	19.7	56	10.81
TiO_2 (6000 rpm)	18.49	52	9.03
TiO_2 (4000 rpm), PCBM 2000 rpm	18.54	71	13.42
TiO_2 (4000 rpm), PCBM 4000 rpm	21.42	67	15.06
TiO_2 (4000 rpm), PCBM 6000 rpm	21.96	71	16.37

Indeed, the presence of PCBM enhances the compactness of ETL, resulting in higher FF and PCE values. Increasing 2000 rpm to 6000 rpm for PCBM with TiO_2 sample (4000 rpm) increases Jsc from 18.54 mA/cm^2 to 21.96 mA/cm^2, resulting in a further increase of PCE from 13.42% to 16.37% (≈ 22% increase). According to the AFM analysis [100], this can be attributed to the observed pinhole-free TiO_2 with the smallest surface roughness value.

In p-i-n structured PSCs, ZnO-added PCBM can serve as ETL. [101] ZnO has been added to PCBM to improve the electrical transfer and heat transfer process. Indeed, ZnO changed the energy level when added to the PCBM film. Experimental results showed that thermal conductivity has improved about 7.4% (6.57 volume) and 23.5% (22.38 volume), respectively. Higher PCE (16.51% to 17.97%), FF (68.81% to 73.58%), V_{oc} (1.04 to 1.06 V) and J_{sc} (23 mA/cm2) were found in 0.05 weight%/ZnO/PCBM and 0.1 weight% /ZnO/PCBM if compared to PCBM sample. Based on PL studies, the PL intensity has been reduced, and the lifetime decreases (80 ns to 34 ns) when ZnO is added. This phenomenon is due to the increase in charge dissociation and electron extraction.

4.2.4. Development of HTL through Doping/Additives

The HTL plays a vital role in hole extraction and electron blocking, thereby enhancing the PCE of PSCs. The common HTLs are spiro-OMeTAD, PEDOT: PSS and NiO. However, Spiro-OMeTAD has inherent stability problem, [29] PEDOT: PSS has low work function and conductivity as well as the polarity mismatch problem with perovskites, [102] and NiO has band alignment mismatch and low conductivity problems. [103] Various additive materials are reported in the literature to improve the performance of these HTLs. Nitrogen-rich porous carbon (NPC), [104] Co(III)-grafted CN nanosheets ($CoCN_2$), [105] Sb_2S_3, [106] SnS nanoparticles [107] and $PbSO_4(PbO)_4$ quantum dots (QDs) [108] are reported (Table 10) as useful additives to improve the stability of Spiro-OMeTAD. The Spiro-OMeTAD HTL-based PSC with $CoCN_2$ additive reached a PCE of 23.01%. [105] Diluted PEDOT: PSS, [109] doping with sodium citrate, [110] and urea as an additive [111] have been reported to enhance the PCE of the PSCs based on PEDOT: PSS HTL. The highest achieved PCE is 18.8% with urea additives [111]. For NiO HTL, cobalt (Co) and rubidium (Rb) doping can reduce the band alignment problem. Reported PCEs of the PSCs with Co and Rb-doped NiO as HTL are 17.77% [112] and 21.8%, [113] respectively (Table 10).

Recently, Elang and co-workers [114] reported CuSCN as a prospective HTL due to its higher hole mobility and higher energy levels than perovskite. The significantly elevated conduction band level of CuSCN (-1.3 eV) as compared with that of the perovskite (-3.75 ev), as shown in Figure 5, effectively ceases electrons to transport to the FTO electrode. Moreover, the valence band level of CuSCN (-5.1

eV) is in between that of the perovskite (-5.43 eV) and the energy level of the FTO electrode (-4.4eV), which eases holes to transport to FTO. The effects of different carbon-based electrodes, i.e. carbon nanotube (CNT), graphite and reduced graphene oxide (rGO), were also investigated by Elang and co-workers. [84] Raman spectroscopy observation reveals two major peaks: the G-band (1590 cm^{-1}) represents the C-C bond, and the D-band (1300 cm^{-1}) is attributed to the disordered graphitic materials. The intensity ratio between these bands, also called as ID/IG ratio, represents the electrical conductivity behavior.

The highest ID/IG ratio of 1.22, as observed in Table 11, between the CNT and CuSCN samples, represents excellent electrical conductivity behaviors. Also, the lowest series resistance, R_s (76.69 Ω observed in Table 11) for these samples, can be attributed to the effective charge movement that occurred from perovskite to the carbon layer. The highest J_{sc} of 0.199 mA/cm^2, observed in Table 11, indicates the high conductivity of multi-walled CNT. Also, the higher FF, PCE, $J_{sc,}$ and V_{oc} (Table 6) in these samples confirm that the recombination process has been reduced, and the charge mobility has been increased.

Table 10. Performance metrics of PSCs are based on different HTLs with additives/doping

HTL	Spiro-OMeTAD					PEDOT: PSS			NiO	
Additive / Doping	NPC	Co (III)-CN	Sb_2S_3	SnS	$PbSO_4(PbO)_4$ QDs	Diluted	Citrate	Urea	Co	Rb
Ref.	[104]	[105]	[106]	[107]	[108]	[109]	[110]	[111]	[112]	[113]
PCE (%)	18.51	23.01	22.13	22.59	22.66	17.85	18.39	18.8	17.77	21.8
FF (%)	76	79.5	79	80.7	80	80.4	75	80.9	79.8	82.4
Voc (V)	1.06	1.138	1.132	1.17	1.142	1.08	1.134	1.03	1.09	1.133
Jsc (mA/cm^2)	23.51	25.43	24.75	24.01	24.8	20.56	21.62	22.57	20.46	23.35

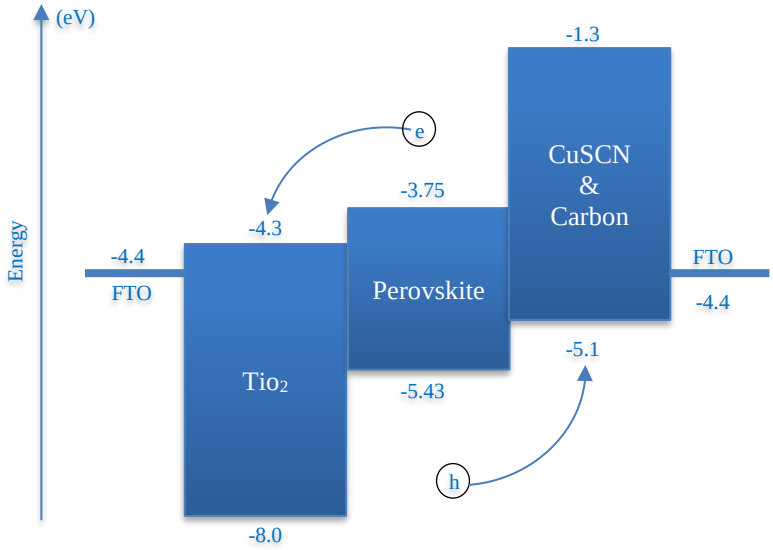

Fig. 5 Energy level diagram in specific solar cells [114]

Table 11. Photovoltaic performance of PSCs with CuSCN as HTL for different electrode materials

PV Performance Metrics	With CNT	With graphite	With rGO
Series resistance, R_s (Ω)	76.69	633	50000
Transfer resistance, R_{trans} (Ω)	2322	3415	0.000001
Recombination resistance, R_{rec} (Ω)	1372	1138	1491
J_{sc} (mA/cm^2)	0.199	0.07	0.019
V_{oc} (V)	0.52	0.36	0.06
FF	0.369	0.348	0.273
PCE (%)	0.0735	0.0168	0.0003
ID/IG ratio	1.22	0.74	0.96

Table 12. PV parameters of plasmonic (Ag NP-based) PSC

Ag NPs for different diameters				
Diameter (nm)	**PCE (%)**	**FF (%)**	**V_{oc} (V)**	**J_{sc} (mA/cm^2)**
5	13.532	82.47	0.9478	17.20868
10	13.644	82.5	0.9478	17.34264
50	14.1537	82.49	0.9447	18.0518
100	13.8525	79.53	0.9307	18.00173
Ag NPs (diameter=25 nm) for different widths				
Width (nm)	**PCE (%)**	**FF (%)**	**V_{oc} (V)**	**J_{sc} (mA/cm^2)**
100	1.4212	0.8175	0.873	15.9061
125	12.2623	0.8381	0.886	16.4142
175	12.6868	0.8206	0.8875	17.4186
200	12.4773	0.8182	0.8879	17.1721
Ag NPs for different temperatures				
Temperature (°C)	**PCE (%)**	**FF (%)**	**V_{oc} (V)**	**J_{sc} (mA/cm^2)**
25	13.5394	0.8202	0.943	17.4
35	13.4815	0.8195	0.94	17.3944
45	13.378	0.8188	0.9336	17.3941
55	13.2877	0.818	0.9282	17.3937
75	13.1073	0.813	0.9213	17.3923

4.2.5. Effects of Silver (Ag) NPs in Plasmonic PSC

The effects of plasmonics on PSCs have been recently investigated by Bahrami and co-workers [115] by employing a Coupled Opto-Electro-Thermal (OET) Modeling. They have investigated carrier transport, thermodynamic properties and opto-electro-thermal behaviors and have observed better photophysics behavior of plasmonic PSCs. They have also studied the influence of Ag NPs in the designed PSC. The diameter and the width of Ag NPs have strong effects on the PV performance metrices. As shown in Table 12, the highest PCE (14.1537%) is obtained when the diameter of Ag NP was 50 nm. For Ag NP with 25 nm diameter, the highest PCE (12.6868%) is obtained for a width of 175 nm. These results reveal that increasing the diameter and width of Ag NPs. However, they have improved performance metrics constrained by a maximum limit, which can be due to the increased thermal losses beyond this limit. The material properties, such as band gap and carrier lifetime, are strongly affected by temperature. The reduction in V_{oc} and J_{sc} observed in Table 12 when the temperature is increased can be due to the increase in dark current density, intrinsic carriers, and recombination rate as temperature increases.

5. Conclusion

Many researchers have prepared OSCs and PSCs successfully. PCE was observed to be improved from time to time. Based on the experimental results, the highest PCE was obtained in the optimized conditions.

Funding Statement

One of the authors (M.I.B.C) was supported by United International University, Bangladesh.

Acknowledgments

This research work was financially supported by INTI International University (Ho SM).

References

[1] Ehsanul Kabir et al., "Solar Energy: Potential and Future Prospects," *Renewable and Sustainable Energy Reviews*, vol. 82, no. 1, pp. 894-900, 2018. [CrossRef] [Google Scholar] [Publisher Link]

[2] Pabitra K. Nayak et al., "Photovoltaic Solar Cell Technologies: Analysing the State of the Art," *Nature Reviews Materials*, vol. 4, pp. 269-285, 2019. [CrossRef] [Google Scholar] [Publisher Link]

[3] Nathan S. Lewis, and Daniel G. Nocera, "Powering the Planet: Chemical Challenges in Solar Energy Utilization," *Proceedings of the National Academy of Sciences*, vol. 103, no. 43, pp. 15729-15735, 2006. [CrossRef] [Google Scholar] [Publisher Link]

[4] Ghazi Aman Nowsherwan et al., "Numerical Optimization and Performance Evaluation of ZnPC: PC70BM Based Dye-Sensitized Solar Cell," *Scientific Reports*, vol. 13, pp. 1-16, 2023. [CrossRef] [Google Scholar] [Publisher Link]

[5] M. Sojoudi et al., "Achieving Steady and Stable Energy from AlGaAsGaAs Solar Cells," *Engineering, Technology & Applied Science Research*, vol. 1, no. 6, pp. 151-154, 2011. [CrossRef] [Google Scholar] [Publisher Link]

[6] A.M. Mouafki et al., "Porous Silicon Antireflective Coatings for Silicon Solar Cells," *Engineering, Technology & Applied Science Research*, vol. 12, no. 2, pp. 8354-8358, 2022. [CrossRef] [Google Scholar] [Publisher Link]

[7] Muhammad Tawalbeh et al., "Environmental Impacts of Solar Photovoltaic Systems: A Critical Review of Recent Progress and Future Outlook," *Science of the Total Environment*, vol. 759, 2021. [CrossRef] [Google Scholar] [Publisher Link]

[8] Askari Mohammad Bagher, Mirzaei Mahmoud Abadi Vahid, and Mirhabibi Mohsen, "Types of Solar Cells and Application," *American Journal of Optics and Photonics*, vol. 3, no. 5, pp. 94-113, 2015. [CrossRef] [Google Scholar] [Publisher Link]

[9] Pranavamshu Reddy et al., "Status of BIPV and BAPV System for Less Energy-Hungry Building in India—A Review," *Applied Sciences*, vol. 10, no. 7, pp. 1-24, 2020. [CrossRef] [Google Scholar] [Publisher Link]

[10] Aritra Ghosh, "Potential of Building Integrated and Attached/Applied Photovoltaic (BIPV/BAPV) for Adaptive Less Energy-Hungry Building's Skin: A Comprehensive Review," *Journal of Cleaner Production*, vol. 276, 2020. [CrossRef] [Google Scholar] [Publisher Link]

[11] Priyanka Roy et al., "Perovskite Solar Cells: A Review of the Recent Advances," *Coatings*, vol. 12, no. 8, pp. 1-24, 2022. [CrossRef] [Google Scholar] [Publisher Link]

[12] Jiaying Wu, et al., "A Comparison of Charge Carrier Dynamics in Organic and Perovskite Solar Cells," *Advanced Materials*, vol. 34, no. 2, 2022. [CrossRef] [Google Scholar] [Publisher Link]

[13] Abdulaziz S.R. Bati et al., "Next-generation Applications for Integrated Perovskite Solar Cells," *Communications Materials*, vol. 4, pp. 1-24, 2023. [CrossRef] [Google Scholar] [Publisher Link]

[14] Ibtissam Tebbal, and Abdelhak Ferhat Hamida, "Effects of Crossover Operators on Genetic Algorithms for the Extraction of Solar Cell Parameters from Noisy Data," *Engineering, Technology & Applied Science Research*, vol. 13, no. 3, pp. 10630-10637, 2023. [CrossRef] [Google Scholar] [Publisher Link]

[15] Martin A. Green, "Self-Consistent Optical Parameters of Intrinsic Silicon at 300 K Including Temperature Coefficients," *Solar Energy Materials and Solar Cells*, vol. 92, no. 11, pp. 1305-1310, 2008. [CrossRef] [Google Scholar] [Publisher Link]

[16] Muhammad Ahsan Saeed et al., "Indoor Organic Photovoltaics: Optimal Cell Design Principles with Synergistic Parasitic Resistance and Optical Modulation Effect," *Advanced Energy Materials*, vol. 11, no. 27, 2021. [CrossRef] [Google Scholar] [Publisher Link]

[17] Leiping Duan, and Ashraf Uddin, "Progress in Stability of Organic Solar Cells," *Advanced Science*, vol. 7, no. 11, pp. 1-39, 2020. [CrossRef] [Google Scholar] [Publisher Link]

[18] C.W. Tang, "Two-Layer Organic Photovoltaic Cell," *Applied Physics Letters*, vol. 48, no. 2, pp. 183-185, 1986. [CrossRef] [Google Scholar] [Publisher Link]

[19] Sarah Holliday et al., "High-Efficiency and Air-Stable P3HT-Based Polymer Solar Cells with a New Non-Fullerene Acceptor," *Nature Communications*, vol. 7, pp. 1-11, 2016. [CrossRef] [Google Scholar] [Publisher Link]

[20] Jianquan Zhang et al., "Material Insights and Challenges for Non-Fullerene Organic Solar Cells Based on Small Molecular Acceptors," *Nature Energy*, vol. 3, pp. 720-731, 2018. [CrossRef] [Google Scholar] [Publisher Link]

[21] R.N. Marks et al., "The Photovoltaic Response in Poly (p-Phenylene Vinylene) Thin-Film Devices," *Journal of Physics: Condensed Matter*, vol. 6, no. 7, 1994. [CrossRef] [Google Scholar] [Publisher Link]

[22] P.W.M. Blom et al, "Device Physics of Polymer: Fullerene Bulk Heterojunction Solar Cells," *Advanced Materials*, vol. 19, no. 12, pp. 1551-1566, 2007. [CrossRef] [Google Scholar] [Publisher Link]

[23] Denis E. Markov et al., "Accurate Measurement of the Exciton Diffusion Length in a Conjugated Polymer Using a Heterostructure with a Side-Chain Cross-Linked Fullerene Layer," *The Journal of Physical Chemistry A*, vol. 109, no. 24, pp. 5266-5274, 2005. [CrossRef] [Google Scholar] [Publisher Link]

[24] Ary R. Murad et al., "Conducting Polymers for Optoelectronic Devices and Organic Solar Cells: A Review," *Polymers*, vol. 12, no. 11, pp. 1-47, 2020. [CrossRef] [Google Scholar] [Publisher Link]

[25] G. Yu et al., "Polymer Photovoltaic Cells: Enhanced Efficiencies via a Network of Internal Donor-Acceptor Heterojunctions," *Science*, vol. 270, no. 5243, pp. 1789-1791, 1995. [CrossRef] [Google Scholar] [Publisher Link]

[26] M. Hösel, D. Angmo, and F. Krebs, *Organic Solar Cells (OSCs)*, Handbook of Organic Materials for Optical and (Opto) Electronic, Devices Properties and Applications, pp. 473-507, 2013. [CrossRef] [Google Scholar] [Publisher Link]

[27] Frederik C. Krebs, "Fabrication and Processing of Polymer Solar Cells: A Review of Printing and Coating Techniques," *Solar Energy Materials and Solar Cells*, vol. 93, no. 4, pp. 394-412, 2009. [CrossRef] [Google Scholar] [Publisher Link]

[28] Jaewang Park et al., "Controlled Growth of Perovskite Layers with Volatile Alkylammonium Chlorides," *Nature*, vol. 616, pp. 724-730, 2023. [CrossRef] [Google Scholar] [Publisher Link]

[29] Ying Chen et al., "Recent Progress in Perovskite Solar Cells: Status and Future," *Coatings*, vol. 13, no. 3, pp. 1-21, 2023. [CrossRef] [Google Scholar] [Publisher Link]

[30] Matteo Pitaro et al., "Tin Halide Perovskites: From Fundamental Properties to Solar Cells," *Advanced Materials*, vol. 34, no. 1, pp. 1-47, 2022. [CrossRef] [Google Scholar] [Publisher Link]

[31] Nam Joong Jeon et al., "A Fluorene-Terminated Hole-Transporting Material for Highly Efficient and Stable Perovskite Solar Cells," *Nature Energy*, vol. 3, pp. 682-689, 2018. [CrossRef] [Google Scholar] [Publisher Link]

[32] Laura M. Herz, "Charge-Carrier Mobilities in Metal Halide Perovskites: Fundamental Mechanisms and Limits," *ACS Energy Letters*, vol. 2, no. 7, pp. 1539-1548, 2017. [CrossRef] [Google Scholar] [Publisher Link]

[33] Moritz Riede et al., "Organic Semiconductors," *Reference Module in Materials Science and Materials Engineering*, 2018. [CrossRef] [Google Scholar] [Publisher Link]

[34] Fang-Chung Chen, "Organic Semiconductors," *Encyclopedia of Modern Optics (Second Edition)*, vol. 5, pp. 220-231, 2018. [CrossRef] [Google Scholar] [Publisher Link]

[35] Maria Antonietta Loi, and Jan C. Hummelen, "Perovskites under the Sun," *Nature Materials*, vol. 12, pp. 1087-1089, 2013. [CrossRef] [Google Scholar] [Publisher Link]

[36] Hui Li, and Wei Zhang, "Perovskite Tandem Solar Cells: From Fundamentals to Commercial Deployment," *Chemical Reviews*, vol. 120, no. 18, pp. 9835-9950, 2020. [CrossRef] [Google Scholar] [Publisher Link]

[37] M. Riede, B. Lüssem, and K. Leo, "Organic Semiconductors," *Comprehensive Semiconductor Science and Technology*, vol. 4, pp. 448-507, 2011. [CrossRef] [Google Scholar] [Publisher Link]

[38] Anna Yu. Samsonova et al., "Excitonic Enhancement and Excited Excitonic States in $CsPbBr_3$ Halide Perovskite Single Crystals," *Materials*, vol. 16, no. 1, pp. 1-8, 2023. [CrossRef] [Google Scholar] [Publisher Link]

[39] Zhuo Yang et al., "Unraveling the Exciton Binding Energy and the Dielectric Constant in Single-Crystal Methylammonium Lead Triiodide Perovskite," *The Journal of Physical Chemistry Letters*, vol. 8, no. 8, pp. 1851-1855, 2017. [CrossRef] [Google Scholar] [Publisher Link]

[40] Michael P. Hughes et al., "Determining the Dielectric Constants of Organic Photovoltaic Materials Using Impedance Spectroscopy," *Advanced Functional Materials*, vol. 28, no. 32, 2018. [CrossRef] [Google Scholar] [Publisher Link]

[41] V.M Agranovich, V.I Yudson, and P. Reineker, "Hybridization of Frenkel and Wannier–Mott Excitons in Organic-Inorganic Heterostructures. Strong Coupling Regime," *Thin Films and Nanostructures*, vol. 31, pp. 317-353, 2003. [CrossRef] [Google Scholar] [Publisher Link]

[42] Thomas Kirchartz, and Uwe Rau, "Linking Structural Properties with Functionality in Solar Cell Materials – The Effective Mass and Effective Density of States," *Sustainable Energy & Fuels*, vol. 2, no. 7, pp. 1550-1560, 2018. [CrossRef] [Google Scholar] [Publisher Link]

[43] Wolfgang Tress, "Metal Halide Perovskites as Mixed Electronic–Ionic Conductors: Challenges and Opportunities-From Hysteresis to Memristivity," *The Journal of Physical Chemistry Letters*, vol. 8, no. 13, pp. 3106-3114, 2017. [CrossRef] [Google Scholar] [Publisher Link]

[44] Andrés Gómez et al., "Ferroelectricity-Free Lead Halide Perovskites," *Energy & Environmental Science*, vol. 12, no. 8, pp. 2537-2547, 2019. [CrossRef] [Google Scholar] [Publisher Link]

[45] Martin Stolterfoht et al., "Photocarrier Drift Distance in Organic Solar Cells and Photodetectors," *Scientific Reports*, vol. 5, pp. 1-7, 2015. [CrossRef] [Google Scholar] [Publisher Link]

[46] Paul Meredith, and Ardalan Armin, "Scaling of Next Generation Solution Processed Organic and Perovskite Solar Cells," *Nature Communications*, vol. 9, pp. 1-4, 2018. [CrossRef] [Google Scholar] [Publisher Link]

[47] Xiwen Gong, "Contactless Measurements of Photocarrier Transport Properties in Perovskite Single Crystals," *Nature Communications*, vol. 10, pp. 1-7, 2019. [CrossRef] [Google Scholar] [Publisher Link]

[48] Samuel D. Stranks et al., "Electron-Hole Diffusion Lengths Exceeding 1 Micrometer in an Organometal Trihalide Perovskite Absorber," *Science*, vol. 342, no. 6156, pp. 341-344, 2013. [CrossRef] [Google Scholar] [Publisher Link]

[49] Christian M. Wolff et al., "Nonradiative Recombination in Perovskite Solar Cells: The Role of Interfaces," *Advanced Materials*, vol. 31, no. 52, pp. 1-20, 2019. [CrossRef] [Google Scholar] [Publisher Link]

[50] Hui Zheng et al., "Encapsulation of Flexible Organic Solar Cells via Parylene and Alumina Dyads," *Organic Electronics*, vol. 128, 2024. [CrossRef] [Google Scholar] [Publisher Link]

[51] Muh Fadhil Albab et al., "High-Performance Semi-Transparent Organic Solar Cells Driven by the Dipole-Controlled Optoelectrical Response of Bilateral Self-Assembled Monolayer Strategy," *Nano Energy*, vol. 121, pp. 1-11, 2024. [CrossRef] [Google Scholar] [Publisher Link]

[52] Asif Mahmood et al., "Chemical Similarity-Based Design of Materials for Organic Solar Cells: Visualizing the Generated Chemical Space of Polymers," *Materials Today Communications*, vol. 38, 2024. [CrossRef] [Google Scholar] [Publisher Link]

[53] F. Padinger, R.S. Rittberger, and N.S. Sariciftci, "Effects of Postproduction Treatment on Plastic Solar Cells," *Advanced functional Materials*, vol. 13, no. 1, pp. 85-88, 2003. [CrossRef] [Google Scholar] [Publisher Link]

[54] Pavel A. Troshin et al., "Material Solubility-Photovoltaic Performance Relationship in the Design of Novel Fullerene Derivatives for Bulk Heterojunction Solar Cells," *Advanced Functional Materials*, vol. 19, no. 5, pp. 779-788, 2009. [CrossRef] [Google Scholar] [Publisher Link]

[55] Guangjin Zhao et al., "Effect of Carbon Chain Length in the Substituent of PCBM-Like Molecules on Their Photovoltaic Properties," *Advanced Functional Materials*, vol. 20, no. 9, pp. 1480-1487, 2010. [CrossRef] [Google Scholar] [Publisher Link]

[56] Hee Un Kim et al., "Naphthalene-, Anthracene-, and Pyrene-Substituted Fullerene Derivatives as Electron Acceptors in Polymer-Based Solar Cells," *ACS Applied Materials & Interfaces*, vol. 6, no. 23, pp. 20776-20785, 2014. [CrossRef] [Google Scholar] [Publisher Link]

[57] Martijn Lenes et al., "Fullerene Bisadducts for Enhanced Open-Circuit Voltages and Efficiencies in Polymer Solar Cells," *Advanced Materials*, vol. 20, no. 11, pp. 2116-2119, 2008. [CrossRef] [Google Scholar] [Publisher Link]

[58] John A. Mikroyannidis et al., "A Simple and Effective Modification of PCBM for Use as an Electron Acceptor in Efficient Bulk Heterojunction Solar Cells," *Advanced Functional Materials*, vol. 21, no. 4, pp. 746-755, 2011. [CrossRef] [Google Scholar] [Publisher Link]

[59] Youjun He et al., "Polymer Indene−C_{60} Bisadduct: A New Acceptor for High-Performance Polymer Solar Cells," *Journal of the American Chemical Society*, vol. 132, no. 4, pp. 1377-1382, 2010. [CrossRef] [Google Scholar] [Publisher Link]

[60] Youjun He et al., "High-Yield Synthesis and Electrochemical and Photovoltaic Properties of Indene-C_{70} Bisadduct," *Advanced Functional Materials*, vol. 20, no. 19, pp. 3383-3389, 2010. [CrossRef] [Google Scholar] [Publisher Link]

[61] Guangjin Zhao, Youjun He, and Yongfang Li, "6.5% Efficiency of Polymer Solar Cells Based on Poly (3-Hexylthiophene) and Indene-

C_{60} Bisadduct by Device Optimization," *Advanced Materials*, vol. 22, no. 39, pp. 4355-4358, 2010. [CrossRef] [Google Scholar] [Publisher Link]

[62] Yongye Liang et al., "Development of New Semiconducting Polymers for High Performance Solar Cells," *Journal of the American Chemical Society*, vol. 131, no. 1, pp. 56-57, 2009. [CrossRef] [Google Scholar] [Publisher Link]

[63] J. Peet et al., "Efficiency Enhancement in Low-Bandgap Polymer Solar Cells by Processing with Alkane Dithiols," *Nature Materials*, vol. 6, pp. 497-500, 2007. [CrossRef] [Google Scholar] [Publisher Link]

[64] Yongye Liang et al., "Highly Efficient Solar Cell Polymers Developed via Fine-Tuning of Structural and Electronic Properties," *Journal of the American Chemical Society*, vol. 131, no. 22, pp. 7792-7799, 2009. [CrossRef] [Google Scholar] [Publisher Link]

[65] Zhicai He et al., "Enhanced Power-Conversion Efficiency in Polymer Solar Cells Using an Inverted Device Structure," *Nature Photonics*, vol. 6, pp. 591-595, 2012. [CrossRef] [Google Scholar] [Publisher Link]

[66] Sih-Hao Liao et al., "Fullerene Derivative-Doped Zinc Oxide Nanofilm as the Cathode of Inverted Polymer Solar Cells with Low-Bandgap Polymer (PTB7-Th) for High Performance," *Advanced Materials*, vol. 25, no. 34, pp. 4766-4771, 2013. [CrossRef] [Google Scholar] [Publisher Link]

[67] Jing-De Chen et al., "Single-Junction Polymer Solar Cells Exceeding 10% Power Conversion Efficiency," *Advanced Materials*, vol. 27, no. 6, pp. 1035-1041, 2015. [CrossRef] [Google Scholar] [Publisher Link]

[68] Hsiang-Yu Chen et al., "Polymer Solar Cells with Enhanced Open-Circuit Voltage and Efficiency," *Nature Photonics*, vol. 3, pp. 649-653, 2009. [CrossRef] [Google Scholar] [Publisher Link]

[69] Yuhang Liu et al., "Aggregation and Morphology Control Enables Multiple Cases of High-Efficiency Polymer Solar Cells," *Nature Communications*, vol. 5, pp. 1-8, 2014. [CrossRef] [Google Scholar] [Publisher Link]

[70] Jingbo Zhao et al., "Efficient Organic Solar Cells Processed from Hydrocarbon Solvents," *Nature Energy*, vol. 1, 2016. [CrossRef] [Google Scholar] [Publisher Link]

[71] Shanshan Chen et al., "Ultrafast Channel II Process Induced by a 3-D Texture with Enhanced Acceptor Order Ranges for High-Performance Non-Fullerene Polymer Solar Cells," *Energy & Environmental Science*, vol. 11, no. 9, pp. 2569-2580, 2018. [CrossRef] [Google Scholar] [Publisher Link]

[72] Guangye Zhang et al., "Nonfullerene Acceptor Molecules for Bulk Heterojunction Organic Solar Cells," *Chemical Reviews*, vol. 118, no. 7, pp. 3447-3507, 2018. [CrossRef] [Google Scholar] [Publisher Link]

[73] Yuze Lin et al., "Balanced Partnership between Donor and Acceptor Components in Nonfullerene Organic Solar Cells with >12% Efficiency," *Advanced Materials*, vol. 30, no. 16, 2018. [CrossRef] [Google Scholar] [Publisher Link]

[74] Xiaopeng Xu et al., "Realizing Over 13% Efficiency in Green-Solvent-Processed Nonfullerene Organic Solar Cells Enabled by 1,3,4-Thiadiazole-Based Wide-Bandgap Copolymers," *Advanced Materials*, vol. 30, no. 3, 2018. [CrossRef] [Google Scholar] [Publisher Link]

[75] Jingshuai Zhu et al., "Alkoxy-Induced Near-Infrared Sensitive Electron Acceptor for High-Performance Organic Solar Cells," *Chemistry of Materials*, vol. 30, no. 12, pp. 4150-4156, 2018. [CrossRef] [Google Scholar] [Publisher Link]

[76] Jin-Liang Wang et al., "Selenopheno[3,2-*b*]Thiophene-Based Narrow-Bandgap Nonfullerene Acceptor Enabling 13.3% Efficiency for Organic Solar Cells with Thickness-Insensitive Feature," *ACS Energy Letters*, vol. 3, no. 12, pp. 2967-2976, 2018. [CrossRef] [Google Scholar] [Publisher Link]

[77] Hong Nhan Trans et al., "17% Non-Fullerene Organic Solar Cells with Annealing-Free Aqueous MoO_x," *Advanced Science*, vol. 7, no. 21, pp. 1-11, 2020. [CrossRef] [Google Scholar] [Publisher Link]

[78] Qishi Liu et al., "18% Efficiency Organic Solar Cells," *Science Bulletin*, vol. 65, no. 4, pp. 272-275, 2020. [CrossRef] [Google Scholar] [Publisher Link]

[79] Zhenzhen Zhang et al., "Selenium Heterocyclic Electron Acceptor with Small Urbach Energy for As-Cast High-Performance Organic Solar Cells," *Journal of the American Chemical Society*, vol. 142, no. 44, pp. 18741-18745, 2020. [CrossRef] [Google Scholar] [Publisher Link]

[80] Gaoda Chai et al., "Fine-Tuning of Side-Chain Orientations on Nonfullerene Acceptors Enables Organic Solar Cells with 17.7% Efficiency," *Energy & Environmental Science*, vol. 14, no. 6, pp. 3469-3479, 2021. [CrossRef] [Google Scholar] [Publisher Link]

[81] Yong Cui et al., "Single-Junction Organic Photovoltaic Cells with Approaching 18% Efficiency," *Advanced Materials*, vol. 32, no. 19, 2020. [CrossRef] [Google Scholar] [Publisher Link]

[82] Jiali Song et al., "High-efficiency Organic Solar Cells with Low Voltage Loss Induced by Solvent Additive Strategy," *Matter*, vol. 4, no. 7, pp. 2542-2552, 2021. [CrossRef] [Google Scholar] [Publisher Link]

[83] Muheeb Ahmad Alkhalayfeh et al., "Spiky Durian-Shaped Au@Ag Nanoparticles in PEDOT: PSS for Improved Efficiency of Organic Solar Cells," *Materials*, vol. 14, no. 19, pp. 1-11, 2021. [CrossRef] [Google Scholar] [Publisher Link]

[84] Davoud Raeyani, and Asghar Asgari, "Enhancing the Efficiency of Inverted Organic Solar Cells with Treatment Techniques: Numerical and Experimental Study," *International Journal of Energy Research*, vol. 2023, no. 1, pp. 1-24, 2023. [CrossRef] [Google Scholar] [Publisher Link]

[85] Maria Sandzhieva et al., "Organic Solar Cells Improved by Optically Resonant Silicon Nanoparticles," *Nanomaterials*, vol. 12, no. 21, pp.

1-10, 2022. [CrossRef] [Google Scholar] [Publisher Link]

[86] Chieh-Ming Tsai et al., "Transparent Low Moisture Permeable Coating for Perovskite Solar Cell Encapsulation," *Surface and Coatings Technology*, vol. 482, 2024. [CrossRef] [Google Scholar] [Publisher Link]

[87] Siddhi Vinayak Pandey, "The Circuitry Landscape of Perovskite Solar Cells: An In-Depth Analysis," *Journal of Energy Chemistry*, vol 94, pp. 393-413, 2024. [CrossRef] [Google Scholar] [Publisher Link]

[88] Jun Li et al., "Room-Temperature Processed Plasma Activated Nickel Oxide Film for Wide-Bandgap Perovskite Solar Cells," *Solar Energy Materials and Solar Cells*, vol. 269, 2024. [CrossRef] [Google Scholar] [Publisher Link]

[89] Kanij Fatema et al., "Structural and Morphological Properties of Single and Mixed Halide Pb-Based Perovskites," *Advances in Condensed Matter Physics*, vol. 2022, no. 1, pp. 1-7, 2022. [CrossRef] [Google Scholar] [Publisher Link]

[90] Zafar Arshad et al., "Magnesium Doped TiO_2 as an Efficient Electron Transport Layer in Perovskite Solar Cells," *Case Studies in Thermal Engineering*, vol. 26, pp. 1-12, 2021. [CrossRef] [Google Scholar] [Publisher Link]

[91] Ri Xu et al., "Enhanced Performance of Planar Perovskite Solar Cells Using Ce-Doped TiO_2 as Electron Transport Layer," *Journal of Materials Science*, vol. 55, pp. 5681-5689, 2020. [CrossRef] [Google Scholar] [Publisher Link]

[92] Amalraj Peter Amalathas et al., "Concentration-Dependent Impact of Alkali Li Metal Doped Mesoporous TiO_2 Electron Transport Layer on the Performance of $CH_3NH_3PbI_3$ Perovskite Solar Cells," *The Journal of Physical Chemistry C*, vol. 123, no. 32, pp. 19376-19384, 2019. [CrossRef] [Google Scholar] [Publisher Link]

[93] Xiaotao Liu et al., "Low Temperature Zn-Doped TiO_2 as Electron Transport Layer for 19% Efficient Planar Perovskite Solar Cells," *Applied Surface Science*, vol. 471, pp. 28-35, 2019. [CrossRef] [Google Scholar] [Publisher Link]

[94] Sanjay Sandhu et al., "Micro Structurally Engineered Hysteresis-Free High Efficiency Perovskite Solar Cell Using Zr-Doped TiO_2 Electron Transport Layer," *Ceramics International*, vol. 47, no. 10, pp. 14665-14672, 2021. [CrossRef] [Google Scholar] [Publisher Link]

[95] Jin-Bo Wu, Chao Zhen, and Gang Liu, "Photo-Assisted Cl Doping of SnO_2 Electron Transport Layer for Hysteresis-Less Perovskite Solar Cells with Enhanced Efficiency," *Rare Metals*, vol. 41, pp. 361-367, 2022. [CrossRef] [Google Scholar] [Publisher Link]

[96] Jiawu Tian et al., "Low-Temperature-Processed Zr/F Co-Doped SnO_2 Electron Transport Layer for High-Efficiency Planar Perovskite Solar Cells," *Solar RRL*, vol. 4, no. 6, 2020. [CrossRef] [Google Scholar] [Publisher Link]

[97] Qi Liu et al., "Effect of Tantalum Doping on SnO_2 Electron Transport Layer via Low Temperature Process for Perovskite Solar Cells," *Applied Physics Letters*, vol. 115, no. 14, 2019. [CrossRef] [Google Scholar] [Publisher Link]

[98] Zafar Arshad et al., "Enhanced Charge Transport Characteristics in Zinc Oxide Nanofibers via Mg^{2+} Doping for Electron Transport Layer in Perovskite Solar Cells and Antibacterial Textiles," *Ceramics International*, vol. 48, no. 17, pp. 24363-24371, 2022. [CrossRef] [Google Scholar] [Publisher Link]

[99] Zhenyu Pang et al., "Hydrophobic PbS QDs Layer Decorated ZnO Electron Transport Layer to Boost Photovoltaic Performance of Perovskite Solar Cells," *Chemical Engineering Journal*, vol. 439, 2022. [CrossRef] [Google Scholar] [Publisher Link]

[100] Gang Lu et al., "A PCBM-Modified TiO_2 Blocking Layer towards Efficient Perovskite Solar Cells," *International Journal of Photoenergy*, vol. 2017, no. 1, pp. 1-9, 2017. [CrossRef] [Google Scholar] [Publisher Link]

[101] Younghun Jeong et al., "Improved Thermal and Electrical Properties of P-I-N-Structured Perovskite Solar Cells Using ZnO-Added PCBM as Electron Transport Layer," *Materials*, vol. 17, no. 6, pp. 1-10, 2024. [CrossRef] [Google Scholar] [Publisher Link]

[102] Wenbin Han et al., "Recent Progress of Inverted Perovskite Solar Cells with a Modified PEDOT: PSS Hole Transport Layer," *ACS Applied Materials & Interfaces*, vol. 12, no. 44, pp. 49297-49322, 2020. [CrossRef] [Google Scholar] [Publisher Link]

[103] Lin Xu et al., "Inverted Perovskite Solar Cells Employing Doped NiO Hole Transport Layers: A Review," *Nano Energy*, vol. 63, 2019. [CrossRef] [Google Scholar] [Publisher Link]

[104] Xuesong Zhou et al., "Metal–Organic Framework-Derived N-Rich Porous Carbon as an Auxiliary Additive of Hole Transport Layers for Highly Efficient and Long-Term Stable Perovskite Solar Cells," *Solar RRL*, vol. 4, no. 3, 2020. [CrossRef] [Google Scholar] [Publisher Link]

[105] Wei Cao et al., "Redox Engineering of Spiro-OMeTAD Based Hole Transport Layer Enabled by Ultrathin Co(III)-Grafted Carbon Nitride Nanosheets for Stable Perovskite Solar Cells," *Nano Energy*, vol. 104, no. A, 2022. [CrossRef] [Google Scholar] [Publisher Link]

[106] Qing Du, "Spiro-OMeTAD: Sb_2S_3 Hole Transport Layer with Triple Functions of Overcoming Lithium Salt Aggregation, Long-Term High Conductivity, and Defect Passivation for Perovskite Solar Cells," *Solar RRL*, vol. 5, no. 11, 2021. [CrossRef] [Google Scholar] [Publisher Link]

[107] Xiaolu Zheng et al., "Organic-Inorganic Hybrid Hole Transport Layers with SnS Doping Boost the Performance of Perovskite Solar Cells," *Journal of Energy Chemistry*, vol. 68, pp. 637-645, 2022. [CrossRef] [Google Scholar] [Publisher Link]

[108] Jihong Zheng et al., "Perovskite Solar Cells Employing a $PbSO_4(PbO)_4$ Quantum Dot-Doped Spiro-OMeTAD Hole Transport Layer with an Efficiency over 22%," *ACS Applied Materials & Interfaces*, vol. 14, no. 2, pp. 2989-2999, 2022. [CrossRef] [Google Scholar] [Publisher Link]

[109] Xiude Yang et al., "Boosting Performance of Inverted Perovskite Solar Cells by Diluting Hole Transport Layer," *Nanomaterials*, vol. 12, no. 22, pp. 1-11, 2022. [CrossRef] [Google Scholar] [Publisher Link]

[110] Wei Hu et al., "High Open-Circuit Voltage of 1.134 V for Inverted Planar Perovskite Solar Cells with Sodium Citrate-Doped PEDOT:PSS as a Hole Transport," *ACS Applied Materials & Interfaces*, vol. 11, no. 24, pp. 22021-22027, 2019. [CrossRef] [Google Scholar] [Publisher Link]

[111] Hytham Elbohy et al., "Tuning Hole Transport Layer Using Urea for High-Performance Perovskite Solar Cells," *Advanced Functional Materials*, vol. 29, no. 47, 2019. [CrossRef] [Google Scholar] [Publisher Link]

[112] Pei-Huan Lee et al., "High-Efficiency Perovskite Solar Cell Using Cobalt Doped Nickel Oxide Hole Transport Layer Fabricated by NIR Process," *Solar Energy Materials and Solar Cells*, vol. 208, 2020. [CrossRef] [Google Scholar] [Publisher Link]

[113] Mengjiong Chen et al., "Homogeneous Doping of Entire Perovskite Solar Cells via Alkali Cation Diffusion from the Hole Transport Layer," *Journal of Materials Chemistry A*, vol. 9, no. 14, pp. 9266-9271, 2021. [CrossRef] [Google Scholar] [Publisher Link]

[114] Elang Barruna et al., "Material Characteristics and Electrical Performance of Perovskite Solar Cells with Different Carbon-Based Electrodes Mixed with CuSCN," *Journal of Electrical and Computer Engineering*, vol. 2023, no. 1, pp. 1-11, 2023. [CrossRef] [Google Scholar] [Publisher Link]

[115] Mohammad Bahrami, Mehdi Eskandari, and Davood Fathi, "Thermal Analysis of a Plasmonic Perovskite Solar Cell: Using Coupled Opto-Electro-Thermal (OET) Modeling," *International Journal of Energy Research*, vol. 2024, no. 1, pp. 1-17, 2024. [CrossRef] [Google Scholar] [Publisher Link]